Supporting Information for

Designing Stimuli-Responsive and Color-Tunable Indicators via the Coexistence of Dual Emitting Centers

Tengyue Wang [a], Jiaren Du [a] *, Xiaomeng Wang [a], Kai Jiang [a], Panqin Wang [a], Shaoxing Lyu [a], Hengwei Lin [a] *

[a] International Joint Research Center for Photo-responsive Molecules and Materials, School of Chemical and Material Engineering, Jiangnan University, 214122, Wuxi, China;

*Corresponding authors:
Dr. Jiaren Du (jiaren.du@jiangnan.edu.cn)
Prof. Dr. Hengwei Lin (linhengwei@jiangnan.edu.cn)

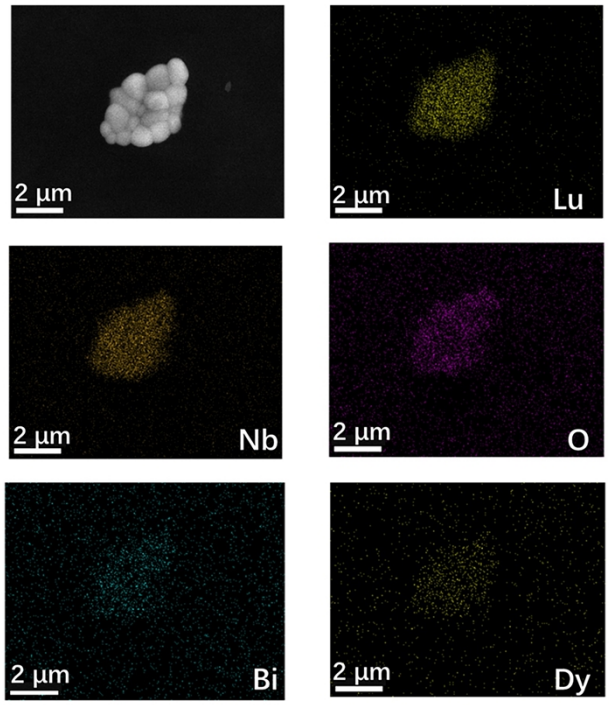

Figure S1. SEM micrograph and their corresponding EDS elemental mappings of $LuNbO_4:Bi^{3+}/Dy^{3+}$ sample.

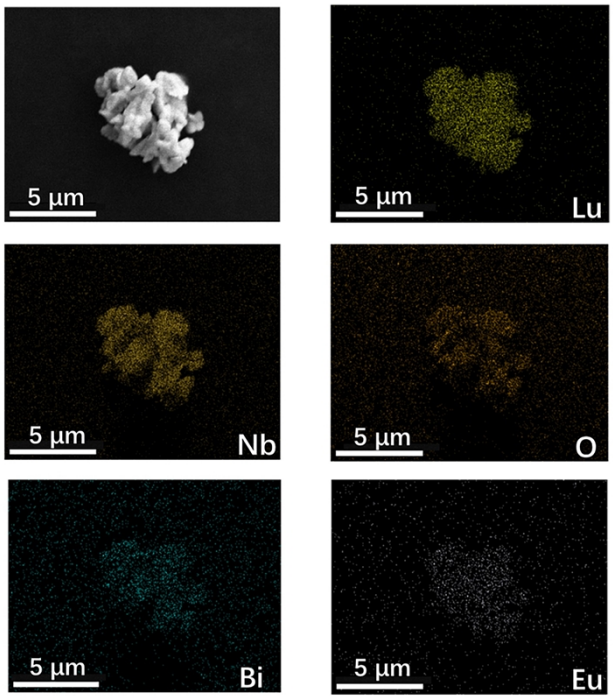

Figure S2. SEM micrograph and their corresponding EDS elemental mappings of $LuNbO_4:Bi^{3+}/Eu^{3+}$ sample.

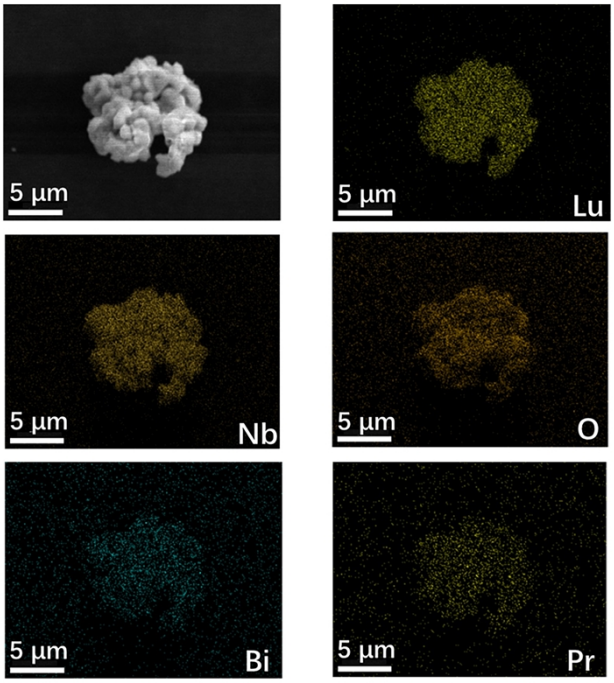

Figure S3. SEM micrograph and their corresponding EDS elemental mappings of $LuNbO_4:Bi^{3+}/Pr^{3+}$ sample.

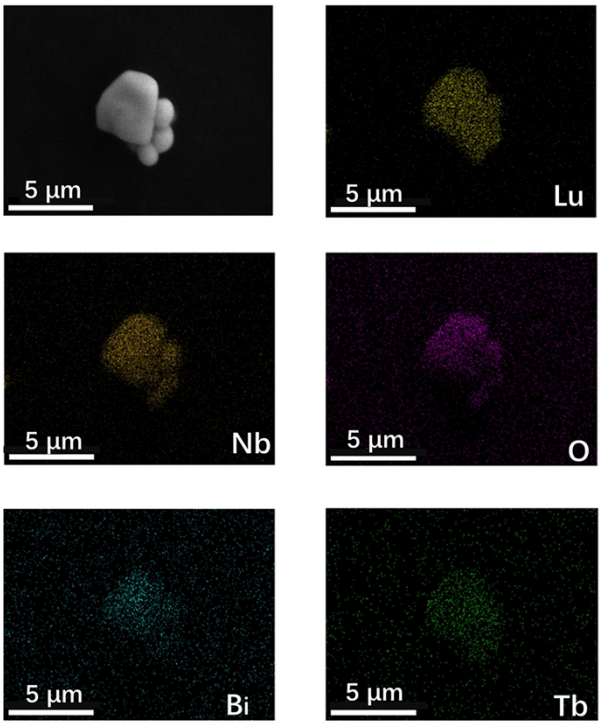

Figure S4. SEM micrograph and their corresponding EDS elemental mappings of $LuNbO_4:Bi^{3+}/Tb^{3+}$ sample.

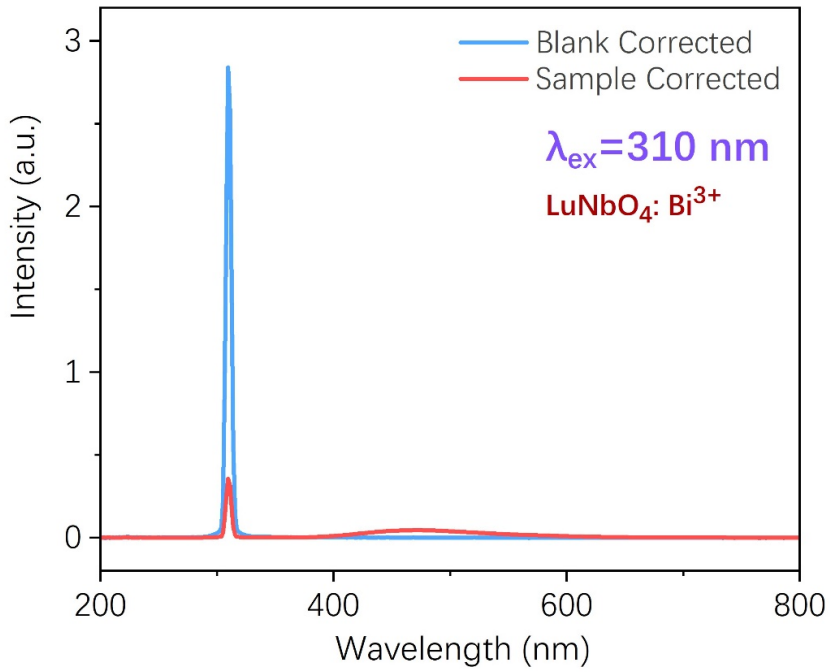

Figure S5. The quantum yield of the optimal $LuNbO_4$:Bi^{3+} sample.

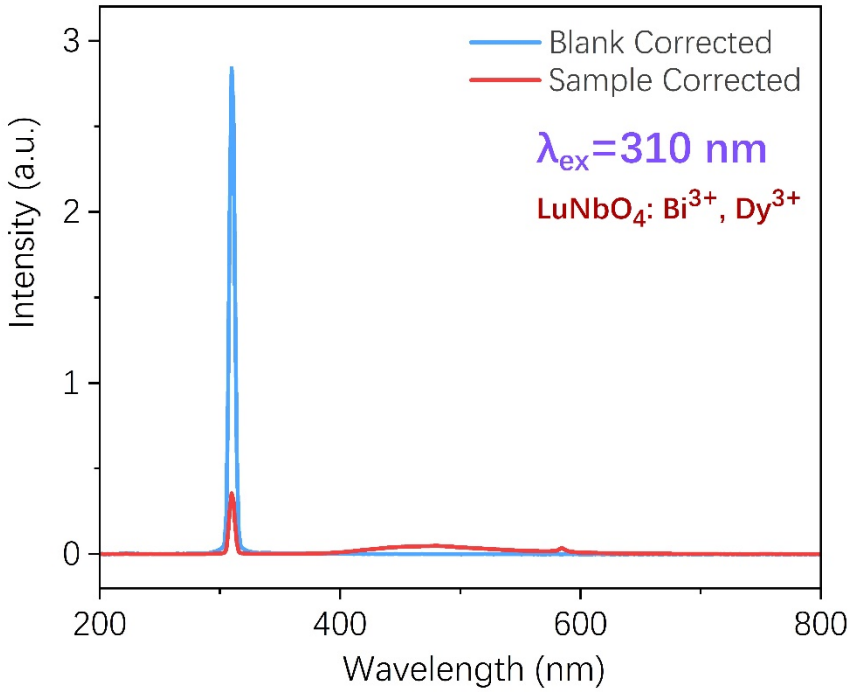

Figure S6. The quantum yield of the optimal $LuNbO_4$:Bi^{3+}, Dy^{3+} sample.

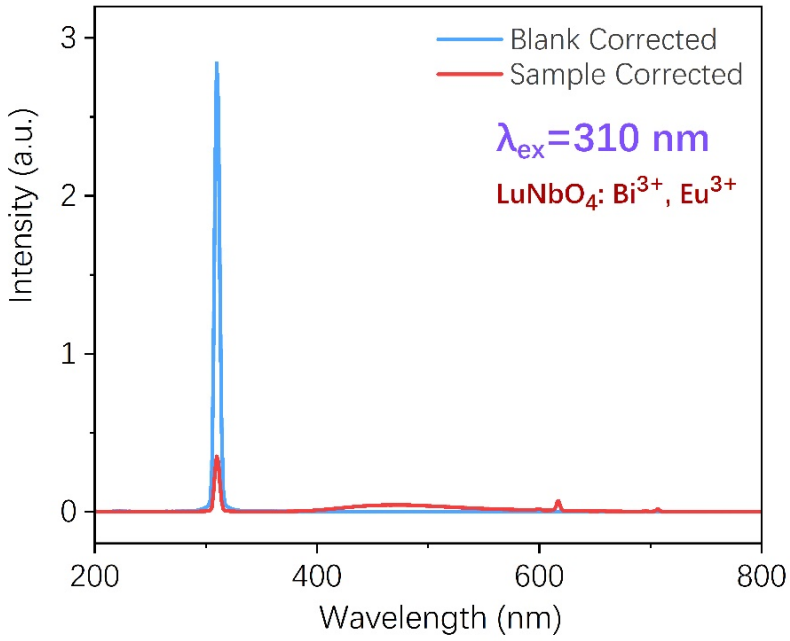

Figure S7. The quantum yield of the optimal $LuNbO_4:Bi^{3+},Eu^{3+}$ sample.

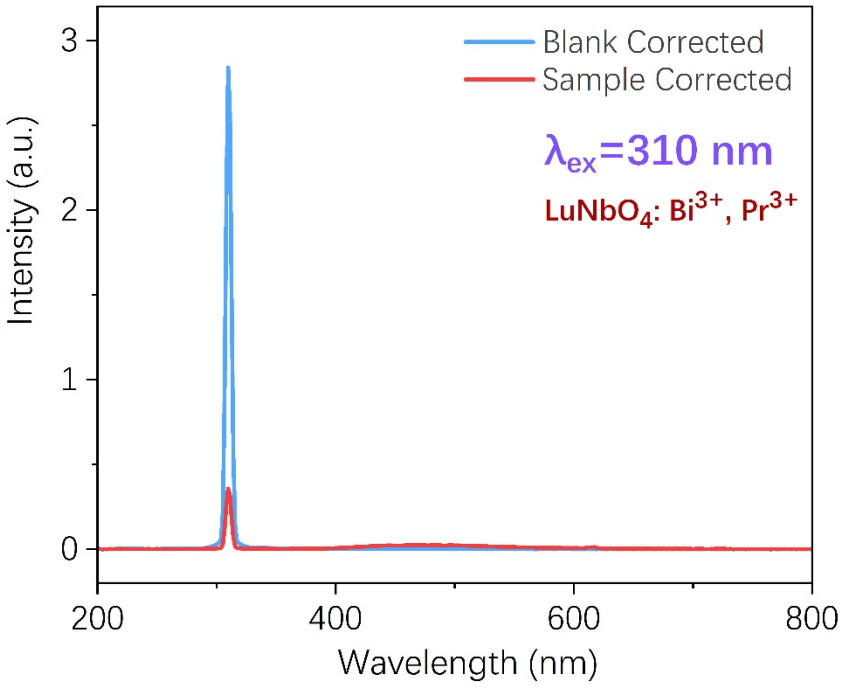

Figure S8. The quantum yield of the optimal $LuNbO_4:Bi^{3+},Pr^{3+}$ sample.

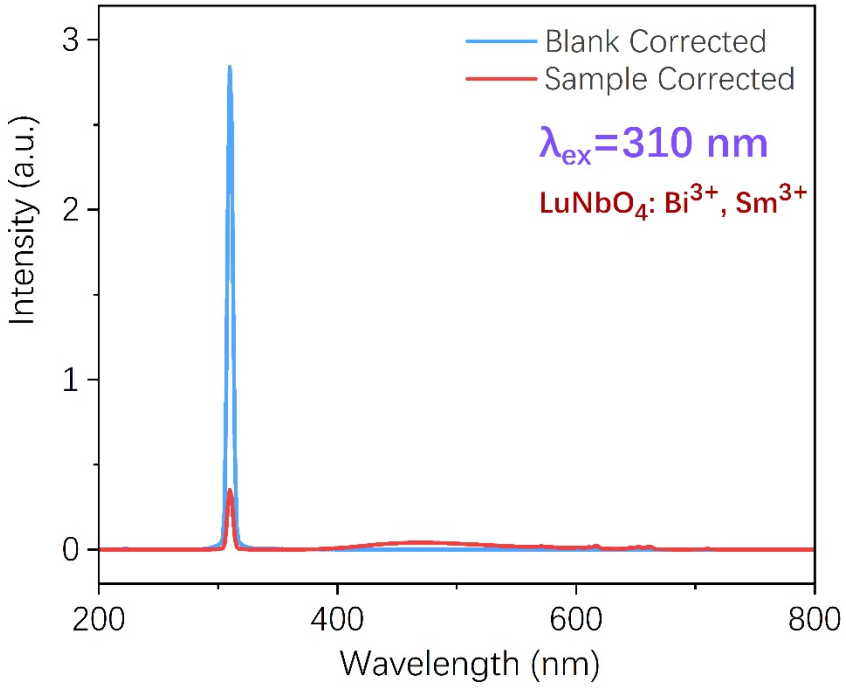

Figure S9. The quantum yield of the optimal $LuNbO_4:Bi^{3+},Sm^{3+}$ sample.

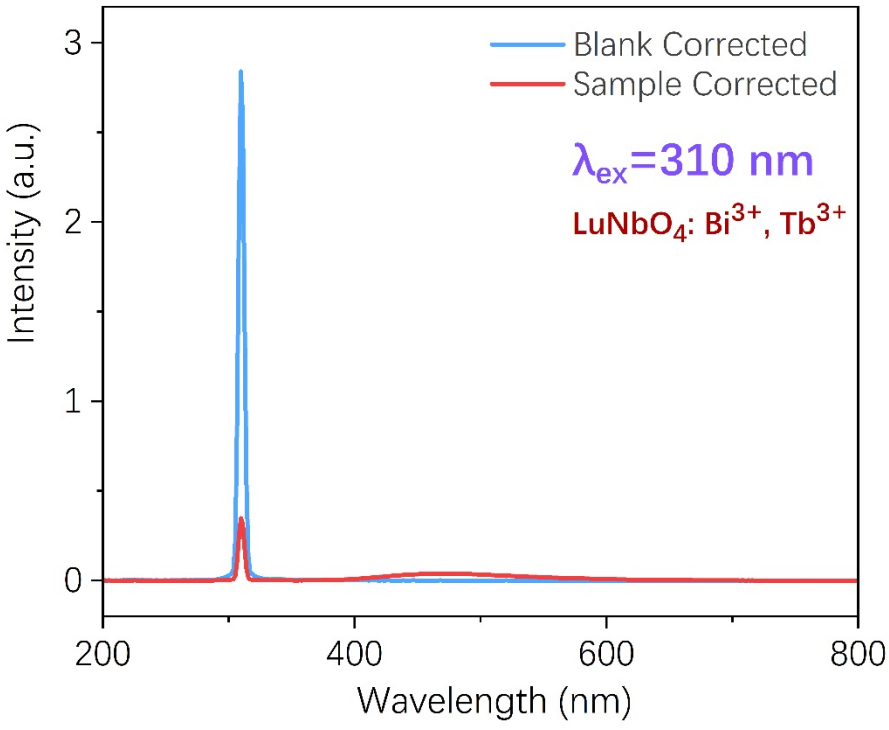

Figure S10. The quantum yield of the optimal $LuNbO_4:Bi^{3+},Tb^{3+}$ sample.

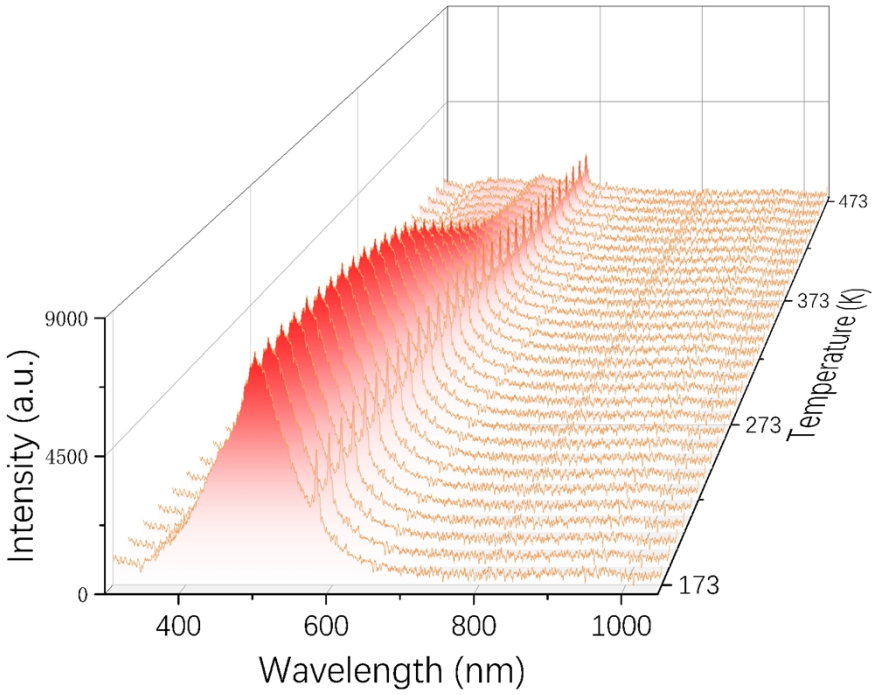

Figure S11. Temperature-dependent PL spectra of $LuNbO_4:Bi^{3+}/Dy^{3+}$ sample from 173 K to 473 K.

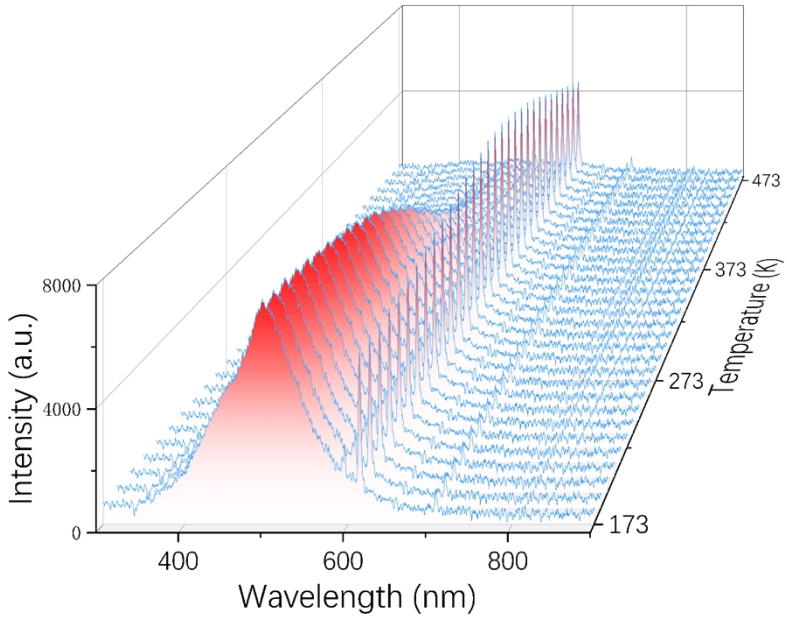

Figure S12. Temperature-dependent PL spectra of $LuNbO_4:Bi^{3+}/Eu^{3+}$ sample from 173 K to 473 K.

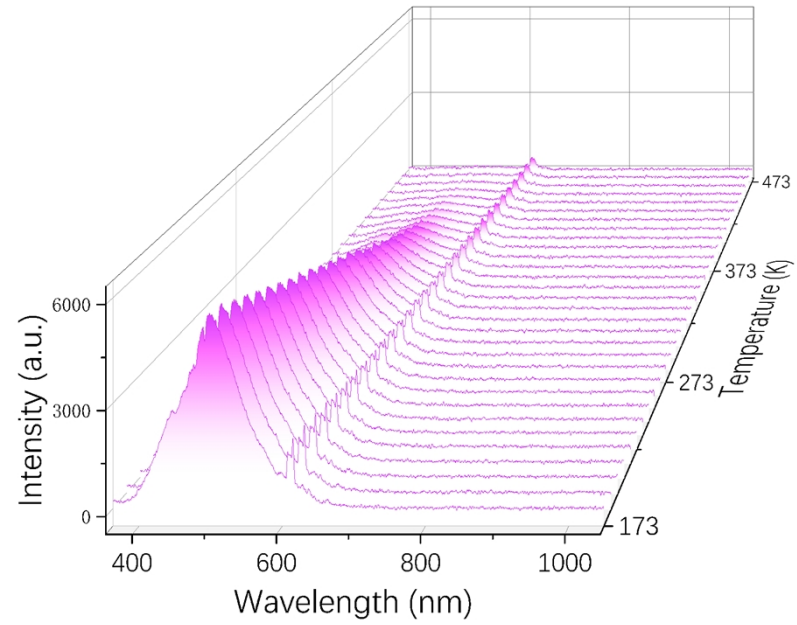

Figure S13. Temperature-dependent PL spectra of $LuNbO_4:Bi^{3+}/Pr^{3+}$ sample from 173 K to 473 K.

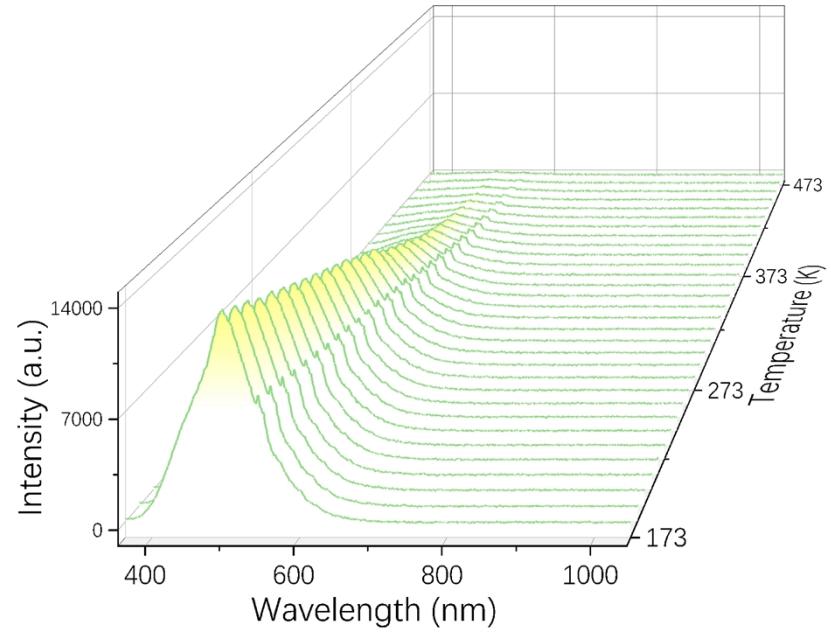

Figure S14. Temperature-dependent PL spectra of $LuNbO_4:Bi^{3+}/Tb^{3+}$ sample from 173 K to 473 K.

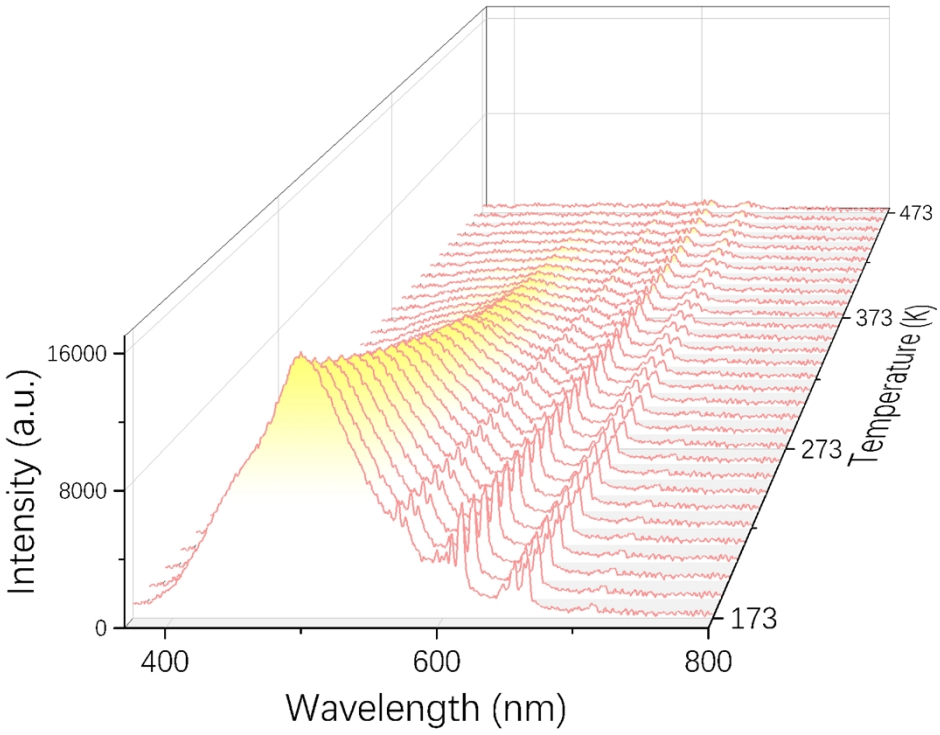

Figure S15. Temperature-dependent PL spectra of $LuNbO_4:Bi^{3+}/Sm^{3+}$ sample from 173 K to 473 K.

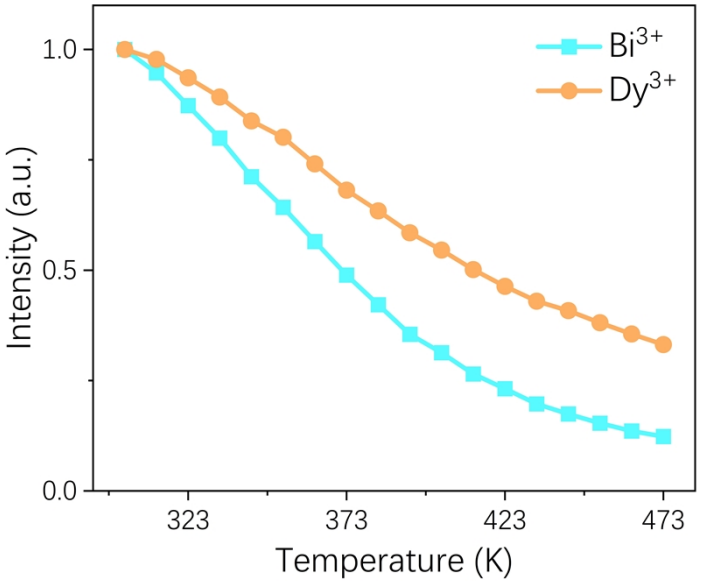

Figure S16. Relative intensity of Bi^{3+} and Dy^{3+} emissions as a function of temperature from the $LuNbO_4:Bi^{3+}/Dy^{3+}$ sample.

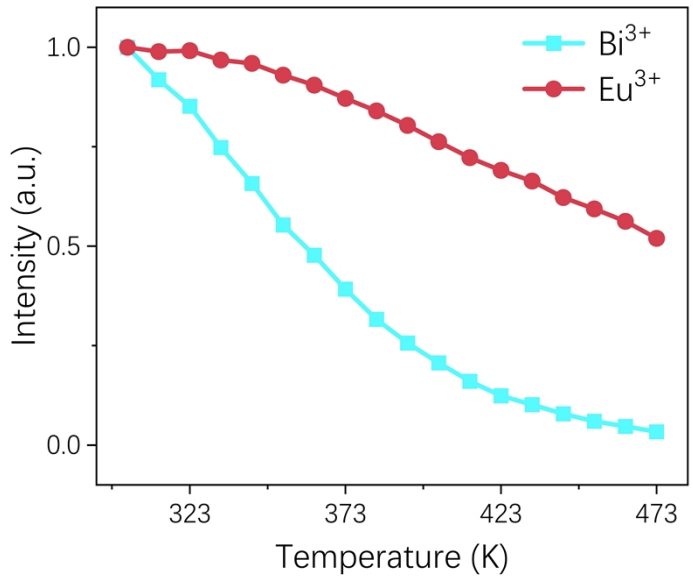

Figure S17. Relative intensity of Bi^{3+} and Eu^{3+} emissions as a function of temperature from the $LuNbO_4:Bi^{3+}/Eu^{3+}$ sample.

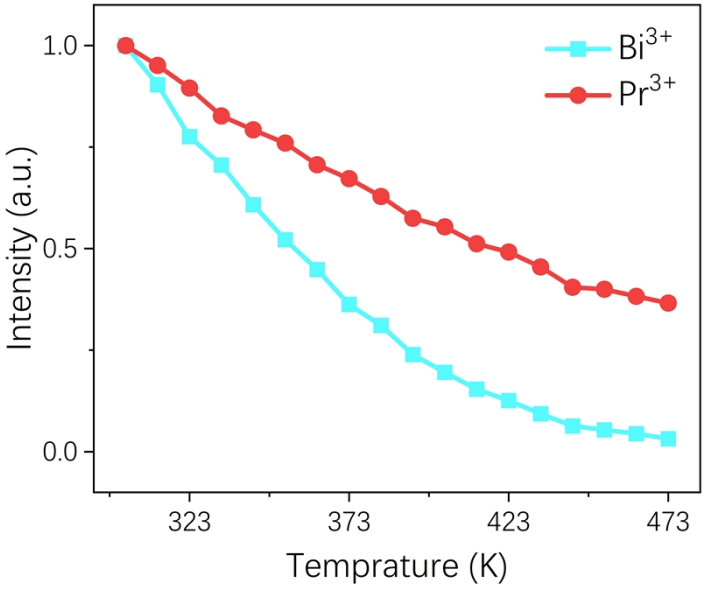

Figure S18. Relative intensity of Bi^{3+} and Pr^{3+} emissions as a function of temperature from the $LuNbO_4:Bi^{3+}/Pr^{3+}$ sample.

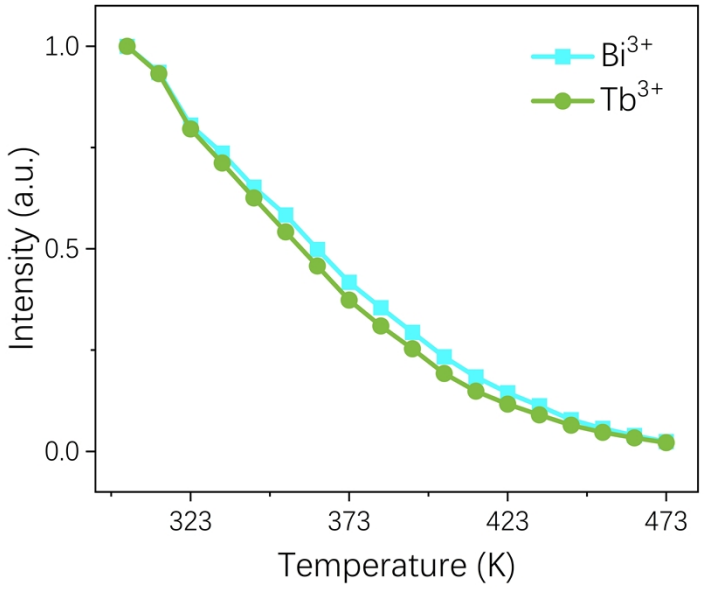

Figure S19. Relative intensity of Bi^{3+} and Tb^{3+} emissions as a function of temperature from the $LuNbO_4:Bi^{3+}/Tb^{3+}$ sample.

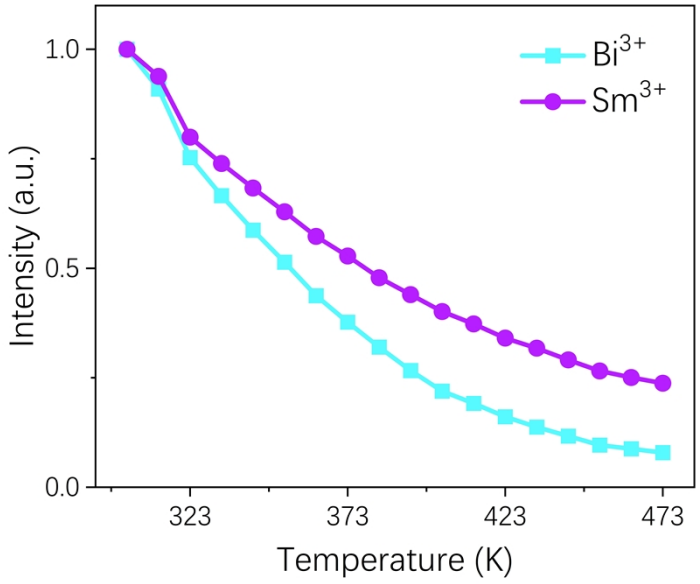

Figure S20. Relative intensity of Bi^{3+} and Sm^{3+} emissions as a function of temperature from the $LuNbO_4:Bi^{3+}/Sm^{3+}$ sample.

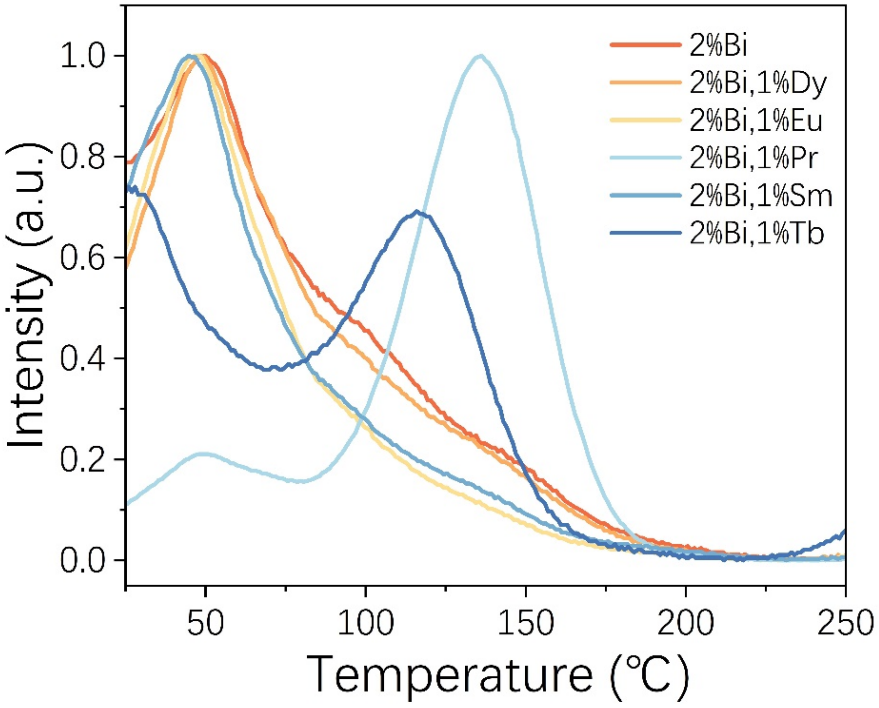

Figure S21. The thermoluminescence curves of $LuNbO_4:Bi^{3+}/Ln^{3+}$ phosphors.

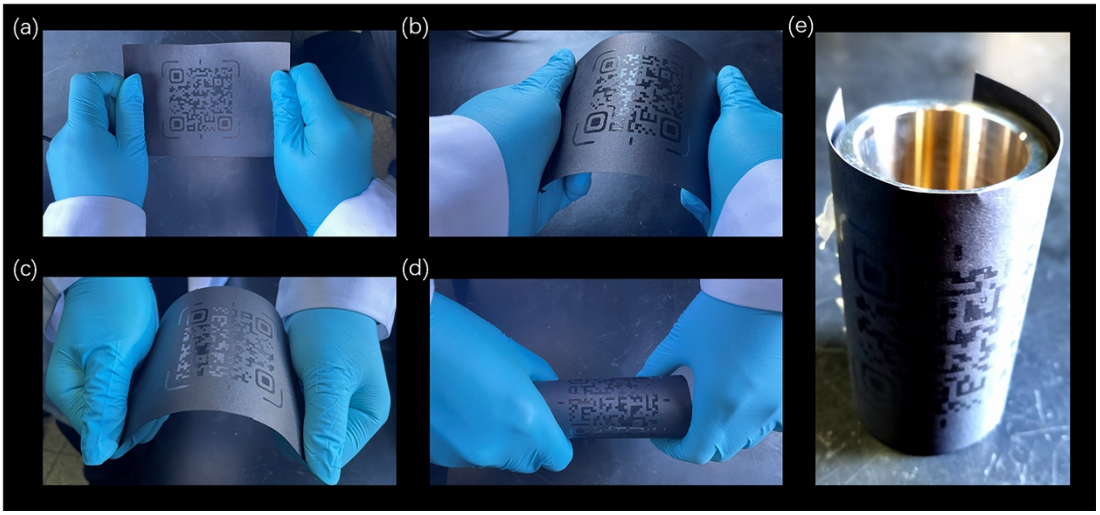

Figure S22. The paper with 2D code was bending (a)-(d), and then attached on the outside surface of a metal cylinder (e).

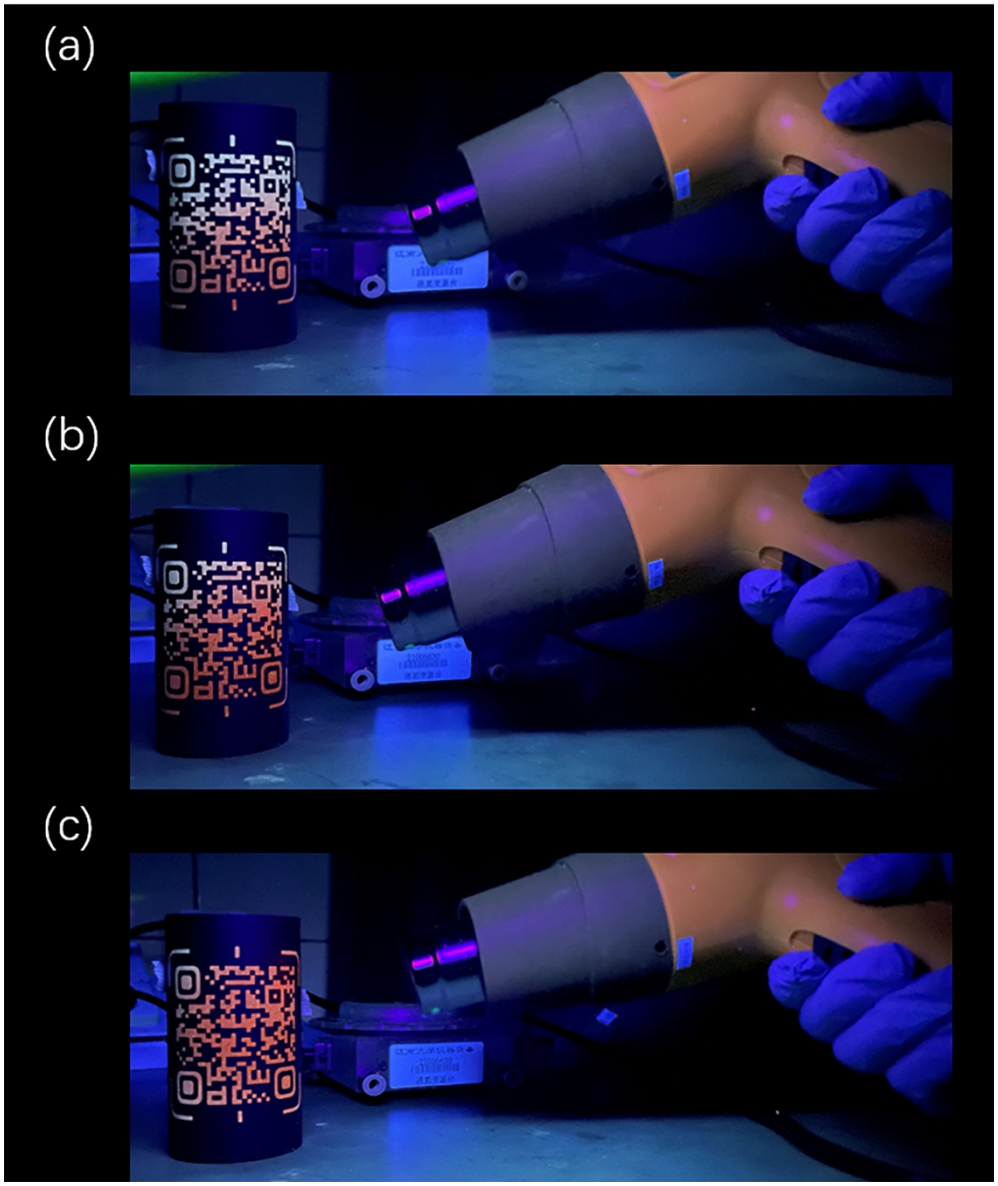

Figure S23. The bending pattern of the 2D code under thermal stimulation from an electric heating gun. (a)-(c) Different heating directions from electric gun (upper end, centrum and lower end) were demonstrated, respectively.

Table S1. The quantum yields of the optimal $LuNbO_4$: Bi^{3+}/Ln^{3+} samples.

Sample	λ_{ex}= 310 nm (QY)
2%Bi^{3+}	65.2%
2%Bi^{3+}, 1%Dy^{3+}	68.8%
2%Bi^{3+}, 1%Eu^{3+}	66.6%
2%Bi^{3+}, 1%Pr^{3+}	37.0%
2%Bi^{3+}, 1%Sm^{3+}	67.2%
2%Bi^{3+}, 1%Tb^{3+}	55.4%